Delayed exciton emission and its relation to blinking in CdSe quantum dots

Freddy T. Rabouw,[1] Marko Kamp,[2] Relinde J. A. van Dijk-Moes,[1] Daniel R. Gamelin,[3] A. Femius Koenderink,[2] Andries Meijerink,[1] and Daniël Vanmaekelbergh[1]

[1]*Condensed Matter and Interfaces, Debye Institute for Nanomaterials Science, Princetonplein 1, 3584 CC Utrecht, The Netherlands*
[2]*Center for Nanophotonics, FOM Institute AMOLF, Science Park 104, 1098 XG Amsterdam, The Netherlands*
[3]*Department of Chemistry, University of Washington, Seattle, Washington 98195–1700, United States*

The efficiency and stability of emission from semiconductor nanocrystal quantum dots (QDs) is negatively affected by 'blinking' on the single-nanocrystal level, i.e. random alternation of bright and dark periods. The timescales of these fluctuations can be as long as many seconds, orders of magnitude longer than typical lifetimes of exciton states in QDs. In this work we investigate photoluminescence from QDs delayed over microseconds to milliseconds. Our results prove the existence of long-lived charge-separated states in QDs. We study the properties of delayed emission as a direct way to learn about charge carrier separation and recovery of the exciton state. A new microscopic model is developed to connect delayed emission to exciton recombination and blinking, from which we conclude that bright periods in blinking are in fact not characterised by uninterrupted optical cycling as often assumed.

I. INTRODUCTION

Blinking, or intermittency, in the photoluminescence (PL) of individual semiconductor nanocrystal quantum dots (QDs) is a fascinating phenomenon that is still not fully understood [1, 2]. Soon after the first observation of blinking in individual QDs [3] the idea was proposed that dark periods were due to temporary charging [4]. Charging would render the QD dark because subsequent excitations would decay not by the emission of a photon but by Auger recombination, i.e. transfer of the recombination energy to the excess charge carrier. This basic idea has been used to develop detailed models for blinking [5–7]. These models have in common that the rates of charging (by charge carrier ejection and trapping) and discharging (by recombination or release of the trapped charge) of the QD fluctuate in time, to understand the surprising power-law statistics of the durations of bright and dark periods. Recent experimental results have put into question the idea that Auger quenching alone can explain the dark periods [8–10]. They support alternative blinking models, where the dark states are due to charge carrier localisation and nonradiative recombination on structural defects in the QD [11–13]. It has also been proposed that blinking can be due to a combination of Auger decay and nonradiative recombination at trap sites [14, 15]. One of the reasons that there is still not one unifying physical model for blinking, is that models are based on rather indirect experimental data, namely the statistics of bright and dark durations.

In this work we examine the PL dynamics of core–shell CdSe/CdS/CdZnS/ZnS QDs over ten orders of magnitude in time. There is exciton recombination on the nanosecond timescale, and blinking on the second timescale. We focus in particular on 'delayed emission' on timescales from microseconds to milliseconds [16, 17]. This component in the PL decay dynamics of QDs is often overlooked because, although its integrated intensity can be higher than 10%, the amplitude is much less than a percent of the exciton emission. We examine the properties of delayed emission, concluding that it is due to charge separation, storage, and eventual recovery of the lowest exciton state. Interestingly, the decay of delayed emission follows a power law, very similar to the statistics of bright and dark durations in blinking. A unifying microscopic model is presented to account for both delayed emission and blinking.

II. RESULTS AND DISCUSSION

Emission dynamics in core–shell quantum dots

The QDs investigated have a CdSe/CdS/CdZnS/ZnS core–shell structure with a 3.4 nm diameter CdSe core, and emit around 630 nm (Figs. 1a,b). Single-QD spectroscopy illustrates the many different dynamical processes that can occur in a QD. The emission intensity trace (Fig. 1c) of a single core–shell QD over a period of 5 min of continued excitation exhibits blinking, i.e. on timescales of up to seconds the QD switches randomly between a state of bright emission (blue shaded area) and states of intermediate brightness (green) or near complete darkness (red). The probability distributions for the duration of bright (ON; blue) and dark (OFF; red) periods (Fig. 1d), obtained with a threshold analysis [5], show that the timescales of the ON/OFF fluctuations range from 10 ms to several seconds. Solid lines are fits to a power-law distribution ($p(t) = t^{-\alpha}$ with t the duration of a period) which yield $\alpha_{\rm ON} = 1.5$ and $\alpha_{\rm OFF} = 1.6$, as typically found for blinking statistics [2, 5, 18].

The PL decay curve of this QD during bright periods (blue data points in Fig. 1e) is single-exponential over two orders of magnitude in intensity with a lifetime of $\tau_{\rm X} = 21$ ns, consistent with the radiative lifetime of the exciton in CdSe QDs. During periods of intermediate intensity (green) or dark periods (red) the PL decay is faster, with fitted lifetimes of 5.5 ns and 0.9 ns, respectively. Such fast decay dynamics are due to non-radiative decay pathways, which have previously been interpreted as Auger recombination of a trion state [4, 19–21] or rapid charge carrier trapping [8, 10, 11] (see below for further discussion).

Clearly, a remarkably wide range of timescales is involved in the emission characteristics of QDs. On the one hand there is the timescale of nanoseconds on which excitations decay (Fig. 1e), while on the other hand there is the timescale of milliseconds to seconds on which the emission intensity fluctuates (Fig. 1d). There are a few papers [16, 17] discussing 'delayed' PL from CdSe QDs on the timescale of up to 1–10 μs. Indeed, on timescales beyond 100 ns the PL decay curve of the bright state in our single QD (Fig. 1f) deviates from the single exponent with the exciton lifetime of $\tau_{\rm X} = 21$ ns (solid line). We can add an exponential 'delayed component' plus background to the fit (dashed line) and obtain a delayed lifetime of $\tau_{\rm d} = 96$ ns. The lifetime of this component is too long to originate from direct radiative recombination of an exciton. In analogy to previous papers [16, 17] we ascribe the delayed emission to exciton storage in a charge-separated state for long periods, before eventual recovery of the delocalised $1S_{3/2}1S_e$ exciton state (i.e. with conduction and valence band states occupied) and emission. In this charge-separated state (at least) one charge carrier is trapped on the surface or in the environment of the QD.

Connecting the nanosecond and millisecond time scales

To further examine the delayed emission dynamics we measure the PL decay of the QD ensemble when dispersed in toluene. On a 100 ns timescale the PL decay of the ensemble (Fig. 2a) looks similar to that of the single QD discussed above. At delay

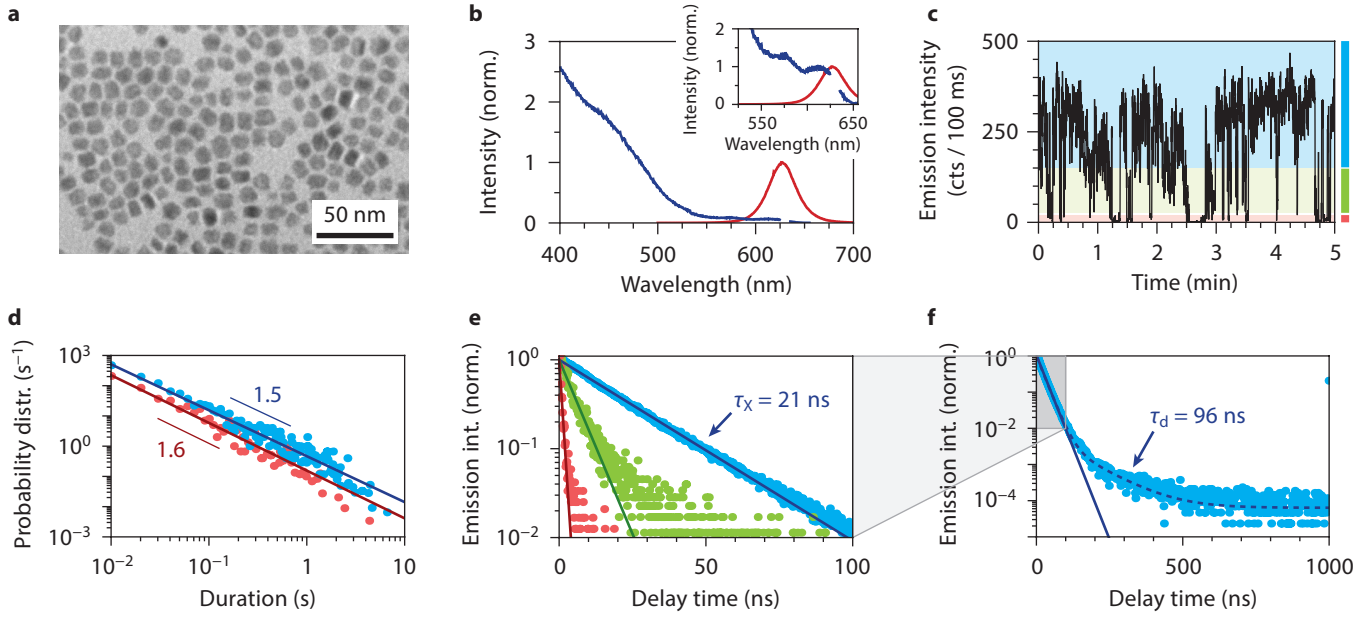

FIG. 1. **Properties of the core–shell quantum dots investigated. (a)** A transmission electron microscopy image of the CdSe/CdS/CdZnS/ZnS core–shell QDs. They have a slightly anisotropic shape of 11.4 ± 1.0 nm by 8.2 ± 0.7 nm (mean $\pm$ standard deviation over 100 QDs) and consist of a CdSe core with a diameter of 3.4 nm, and shells of CdS (6 monolayers), CdZnS (1 monolayer) and ZnS (1 monolayer). **(b)** PL excitation (blue) and emission (red) spectra of the ensemble of QDs. There is a single emission band centered at 630 nm originating from exciton recombination in the CdSe core. The excitation spectrum is dominated by strong absorption by the CdS shell at wavelengths shorter than 500 nm. The inset is a zoom-in, revealing the discrete electronic transitions in the CdSe core. **(c)** An emission intensity trace of a single core–shell QD under continued excitation. The bin size is 100 ms. Coloured shadings indicate the ranges of intensity values which for further analysis are considered bright (blue), intermediate (green), and dark (red). **(d)** The probability distribution of the duration of bright (blue) and dark (red) periods, extracted from the emission intensity trace at a bin size of 10 ms. Solid lines are fits to a power-law trend, from which we obtain exponents of 1.5 for the bright periods, and 1.6 for the dark periods. **(e)** PL decay curves of the bright (blue), intermediate (green), and dark (red) periods, constructed after selecting time bins based on emission intensity. Solid lines are fits to single-exponential decay. We obtain the exciton lifetime of $\tau_X = 21.3$ ns from the bright periods, and PL lifetimes of 5.5 ns and 0.9 ns during the intermediate and dark periods, respectively. With a bin width of 0.165 ns, the absolute peak counts in the PL decay curves are 21.5 (blue), 14.8 (green), and 5.3 (red) cts / 100 ms. **(f)** PL decay curve for the bright periods plotted over a time range of 1 μs. The solid line is the single-exponential fit to the first 100 ns (with $\tau_X = 21.3$ ns; panel **e**). Adding a second exponential decay component and a background yields the dashed line. We obtain a time constant for the delayed component of $\tau_d = 96$ ns. This PL decay curve has a bin width of 1.65 ns, 10$\times$ wider than in **e**.

times longer than 100 ns the decay curve (Fig. 2b) deviates from the double-exponential fit of Fig. 2a (dot-dashed line). In fact, the PL decay follows a power-law over the next four orders of magnitude in time (from $\sim$ 100 ns to 1 ms) and seven orders of magnitude in emission intensity. The power exponents that we fit are similar to those of the blinking statistics (Fig. 1d), namely 1.7 between 200 ns and 400 μs, and 2.0 between 50 μs and 5 ms. Interestingly, the integrated intensity of delayed emission contributes as much as 10%–15% of the total number of emitted photons. This would mean that following excitation there is a 10%–15% probability of charge separation. The observation of delayed emission from several single QDs (Supplementary Figure S2) [16] indicates that the competition between direct and delayed emission happens on the single-QD level, rather than being an ensemble effect.

Figs. 2c,d compare the exciton emission and delayed emission spectra of the ensemble of QDs in toluene. In the first 200 ns (Figs. 2c) after excitation the emission peak shifts to the red, because smaller QDs in the ensemble emitting at shorter wavelengths have a faster radiative decay rate than the larger ones emitting at longer wavelengths [22]. The spectrum of the delayed emission (Fig. 2d) is similar to the exciton emission, but with the emission peak position slightly red shifted by $\sim$ 10 meV (see also Fig. 2e). From this similarity we conclude that delayed emission is the result of recovery of and emission from the delocalised $1S_{3/2}1S_e$ exciton state, rather than direct radiative recombination of charge carriers in the charge-separated state. The red shift of $\sim$ 10 meV of the delayed emission compared to the exciton emission might indicate that in the smaller QDs of the ensemble, i.e. those emitting at shorter wavelengths, charge carrier separation (which eventually leads to delayed emission) is somewhat less likely than in the larger QDs.

To learn more about the process of charge carrier separation, we measured the PL decay of the ensemble of QDs while dispersed in solvents of different refractive indices. Fig. 3a shows how the decay dynamics change when going from a low

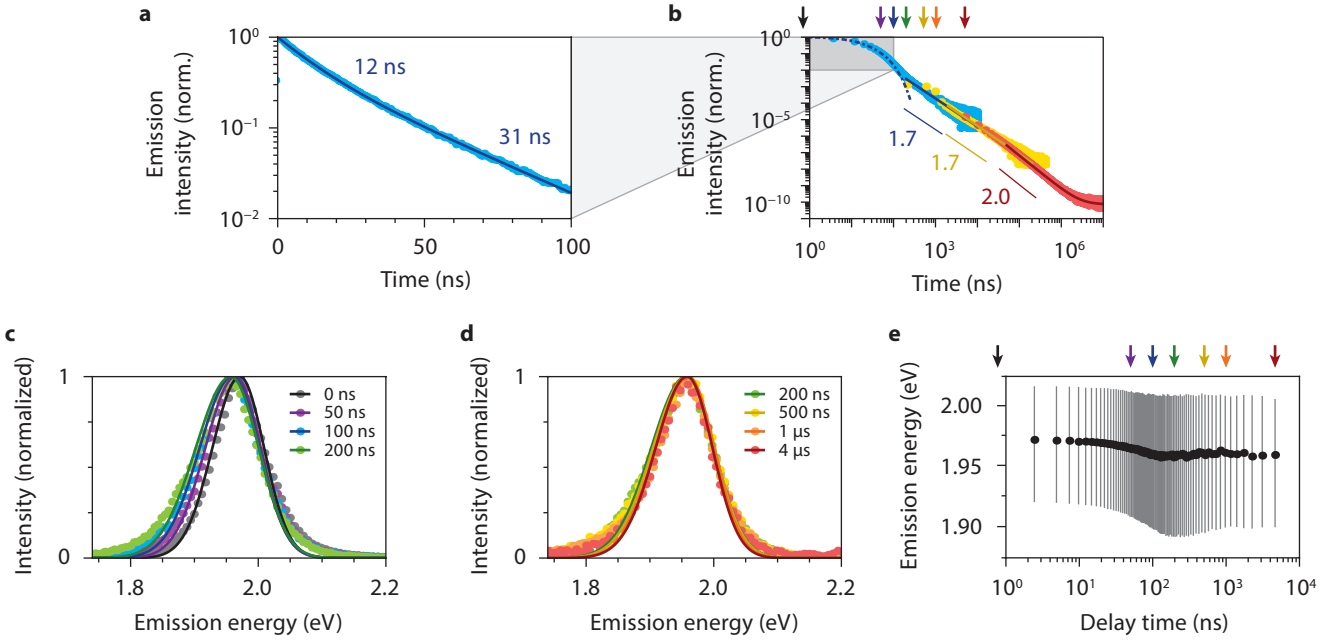

FIG. 2. **Delayed emission after up to milliseconds. (a)** The ensemble PL decay curve of the core–shell QDs appears near exponential on a 100 ns time scale. A biexponential fit yields lifetime components of 17 ns and 31 ns. **(b)** We can measure PL from the ensemble of QDs until up to as long as milliseconds after the laser pulse. On time scales longer than 100 nanoseconds the PL decay clearly deviates from the biexponential behaviour (blue dash-dotted line) fitted to the first 100 ns. Blue, yellow, and red data points are three separate measurements, taken with a diode laser with a repetition rate of 100 kHz (blue), an OPO laser with a repetition rate of 20 Hz (yellow, red). The red curve was taken on a concentrated QD dispersion over a measurement time of 3 days. The PL decay after a delay time of 200 ns can be fitted to power-law decay, yielding a power exponent of 1.7 between 200 ns and 400 μs, and 2.0 between 50 μs and 5 ms. **(c)** The emission spectrum of the ensemble of QDs in toluene at varying time delays after the excitation pulse of 0 (black), 50 (purple), 100 (blue), and 200 (green) ns. The emission peak redshifts over 15 meV and the spectrum becomes broader by 20 meV. The solid lines are fits to a two-sided Gaussian (see Methods). **(d)** The emission spectrum at longer delay times of 200 (green; same as in **c**), 500 (yellow), 1000 (orange), and 4000 (red) ns. The changes occurring in the first 200 ns are partially reversed: the peak blueshifts over 2 meV, and the band width decreases by 10 meV. **(e)** The emission energy (dots) and band width (lines) of the ensemble of QDs as a function of delay time after the excitation pulse, as obtained from two-sided Gaussian fits to the emission spectra (see Methods). Arrows on the top mark the spectra shown in panels **c** and **d**.

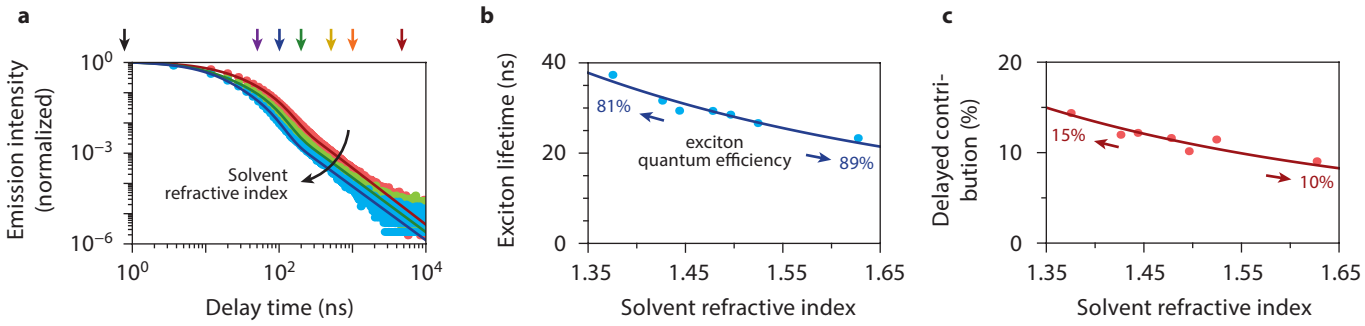

FIG. 3. **Photonic effects on charge carrier trapping. (a)** PL decay curves of the ensemble of QDs over a time scale of 10 μs for different solvents in which they are dispersed: hexane (red; refractive index $n = 1.375$), trichloroethylene (green; $n = 1.478$), and carbon disulfide (blue; $n = 1.627$). Solid lines are fits to decay with a biexponential contribution from direct exciton recombination and a power-law contribution from delayed emission. Arrows on the top mark the delay times for which the spectra are shown in Figs. 2c,d. **(b)** The exciton lifetime [average lifetime from a biexponential fit to the first 100 ns of decay (see Fig. 2a), weighted by integrated intensity] is shorter in solvents with higher refractive index, because the the local density of optical states is higher [23]. From the data we fit that the quantum efficiency of the exciton, i.e. the probability of direct radiative decay, is roughly 80%–90% depending on the refractive index. **(c)** The contribution of power-law delayed emission as a percentage of the total number of photons emitted, as obtained from a fit to Eq. 2. The presence of a trend with solvent refractive index indicates that charge carrier separation happens from the lowest exciton state and competes with direct radiative recombination of the exciton. The solid line is a fit assuming that the rate of charge separation is fixed, while the rate of radiative decay of the exciton changes with the local density of optical states [24].

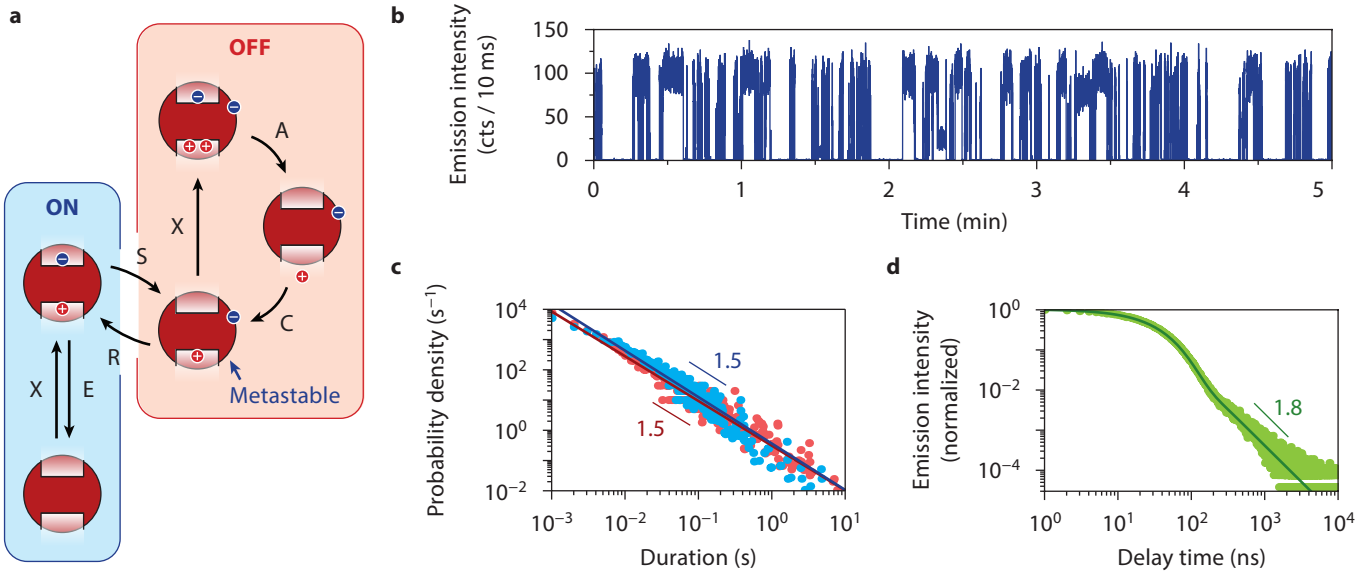

FIG. 4. **Simulation of power-law delayed emission and power-law blinking.** **(a)** In the charging model for blinking, optical cycling (X: excitation, E: emission) in the ON-state (blue panel) is sometimes interrupted by charge carrier separation (S): ejection of a carrier from the QD core and trapping in the environment, e.g. on the surface or in the shell. This leaves the QD with a single delocalised carrier. The QD is then OFF (red panel) because subsequent excitations (X) decay non-radiatively via Auger recombination (A) and charge carrier cooling (C). The QD returns to the ON-state if the delocalised exciton state recovers (R) by release of the trapped carrier. In our model the probability for charge separation P_S is fixed, while the recovery rate γ_R fluctuates strongly over time (see Methods). **(b)** An emission intensity trace simulated with our model for a laser repetition period of 1 μs, an exciton decay rate of $\gamma_X = 1/30$ ns, a probability of charge carrier separation of $P_S = 15\%$, and diffusion and release exponents of $\alpha_d = 1.7$ and $\alpha_r = 1.55$ (see Methods). **(c)** The durations of bright and dark periods are power-law distributed, although there is a deviation in the bright statistics for durations shorter than 10 ms. **(d)** The histogram of delay times shows an exponential component originating from direct exciton recombination and a power-law delayed component. From a fit to Eq. 2 we obtain a power exponent of $\alpha = 1.8$, and recover the input values of $P_S = 15.4\%$ and $\gamma_X = 1/29.7$ ns.

refractive index (hexane; red; $n = 1.375$) to a high refractive index solvent (carbon disulphide; blue; $n = 1.627$). Solid lines are fits (see Methods). The average PL lifetime of the exciton becomes longer at lower refractive index (Fig. 3b) because radiative decay is slower in a medium with lower refractive index, as described by the nanocrystal-cavity model [23]. From the data of Fig. 3b we estimate that the quantum efficiency of direct exciton emission is around 80%–90% (see Methods). This is consistent with a significant probability of charge separation.

Fig. 3c shows that the relative contribution of the delayed component as a percentage of the total emission intensity is lower if the refractive index of the solvent is higher. This is the result of competition between charge carrier separation and direct exciton emission from the same excited state. If in a high refractive index solvent the rate of radiative decay from the exciton state is enhanced, then the probability of separation is reduced [24]. Hence, we must conclude that charge carrier separation occurs from the lowest-energy exciton state of our QDs (i.e. the emitting one), not from hot carrier states as previously proposed to explain so-called B-type blinking [14]. In fact, our model presented below provides an alternative but natural explanation for B-type blinking [14] (see Supplementary Figure S3).

Monte Carlo simulation of blinking and delayed emission

The similarity in power-law statistics for blinking (Fig. 1f) and delayed emission (Fig. 2b) suggests that the same physical process underlies the two phenomena. Can delayed emission be explained in terms of existing models for blinking [2]? A model for blinking must at least contain (1) an explanation for the power-law statistics of ON and OFF durations, and (2) a microscopic picture for the dark state. Based on the early paper of Efros & Rosen [4], most models are 'charging models' (Fig. 4a). They ascribe the dark periods to temporary charging of the QD. The excess charge carrier quenches emission by enabling Auger recombination (step A in Fig. 2c). Alternative 'fast trapping models' [11, 12] propose that the QD becomes dark when fluctuations in the QD structure open nonradiative recombination pathways via trap states.

Only models based on charging are consistent with the observation of delayed emission on time scales from 100 ns to 1 ms (Fig. 2b), because delayed emission requires a long-lived metastable electronically excited state only present in charging models [5–7] (highlighted in Fig. 4a). In existing charging models for blinking this is a long-lived charge-separated state with one

delocalised and one trapped charge. The release rates for the trapped charge fluctuate widely in time, to explain the power-law distribution in OFF durations (Fig. 1d). These wide fluctuations would also lead to power-law decay of the delayed emission (Fig. 2b). We therefore conclude that our observation of delayed emission over long timescales supports a charging model for blinking, involving long-lived charge-separated states.

Recently, in specially designed core–shell structures a 'gray state' with 10%–40% intensity has been often observed in the blinking traces. It could be identified as a *negatively* charged state [15, 26], with exponential blinking statistics [14, 27] rather than power-law. The dynamics of this gray state are consistent with those of the negative trion state created electrochemically [14, 28] or photochemically [29]. However, in most QDs a dark state (rather than a gray state) is dominant in the blinking trace. This darkest state (which comes with power-law statistics [27]) has recently been proposed by Park *et al.* [25] to involve ejection and trapping of an electron, leaving the QD with an excess *positive* charge in the valence band. We therefore identify the trapped charge in the charge-separated state involved in power-law blinking and delayed emission as the electron (as depicted in Fig. 4a). Indeed, positive trions (consisting of an exciton plus the excess hole) created in the charge-separated dark state exhibit much faster Auger decay than negative trions involved in the gray state [25, 29], explaining that the charge-separated state is dark. Alternatively, to explain apparent discrepancies at the single-QD level between the decay rate of the dark state in blinking and the biexciton decay rate [9], one might assume that the excess hole localises at a defect or surface site. Indeed, also localised charge carriers can enable rapid Auger quenching [30].

At first sight delayed emission seems to fit in existing charging models for blinking, which propose long-lived charge-separated states [5–7]. There is however one important feature of delayed emission that is not properly accounted for in existing models, namely that the integrated intensity amounts to as much as 10%–15% of the total emission. The models explain the long ON times that occur (see Fig. 1d) in terms of unperturbed optical cycling (processes X,E in Fig. 2c). In these models charge carrier separation is sometimes prevented for long periods, for example by fluctuating tunnelling barriers and heights [5], Coulomb blockade [6], or diffusion of the relative energies of the exciton state and the charge-separated state [7]. If optical cycling went indeed unperturbed for milliseconds or even seconds as existing models suggest, the relative contribution of the delayed emission could never become 10%–15% of the total emission (see Supplementary Fig. S4).

We have developed a simple model (Fig. 3a) for blinking that simultaneously explains the (power-law distributed) ON and OFF durations of seconds in the intensity trace of a single QD (Fig. 1c), and the significant contribution of delayed emission to the total emission (Fig. 2b). In its simplest form the model assumes a single trap that can cause charge separation by trapping an excited charge carrier, rendering the QD dark due to Auger quenching by the remaining carrier. The key ingredients of the model are that (1) the probability of charge carrier separation is fixed at a few percent (determined by competition with radiative decay; Fig. 3), that (2) the exciton recovery rate is constant only during a power-law distributed time T, and that (3) after time T the recovery rate changes to a random new value such that the time-averaged distribution of recovery rates follows a power-law [5–7]. Power-law distributed times T would naturally follow from a microscopic picture that charge separation involves charge carrier trapping on a structural defect or a particular arrangement of the organic ligand shell, and that energetic barriers for structural changes are exponentially distributed. For details of the model see the Methods section.

The most radical difference with existing blinking models is the assumption that at all times there is a finite probability of charge separation (which we assume fixed, but it can also be allowed to fluctuate around some mean value). This assumption ensures that the delayed emission has a sufficiently high integrated intensity, and is supported by our finding that the contribution of delayed emission increases with decreasing refractive index (Fig. 3). However, the assumption implies that long ON periods are in fact not characterised by unperturbed optical cycling, as currently assumed. Instead, they occur when for a long period T the exciton recovery rate is much faster than the excitation rate. The QD is then 'effectively ON', i.e. optical cycling is interrupted by OFF periods so short (i.e. ns – μs) that they do not affect the emission intensity during period T. Note that these short OFF periods are however responsible for the delayed emission that we observe in the PL decay traces of single QDs (Fig. 1f and Supplementary Fig. S2). Figs. 3b,c,d present the results of a Monte Carlo simulation of the emission dynamics in a QD using our model. The intensity trace (Fig. 3b) and distributions of ON and OFF durations (Fig. 3c) are as typically encountered for single QDs. At the same time, the PL decay curve (Fig. 3d) contains a power-law delayed component with a relative contribution of 15%. Hence, our new model successfully reproduces the most important aspects of the emission dynamics of QDs.

Conclusion

To summarize, we have observed delayed emission from semiconductor QDs as direct evidence for the existence of a charge-separated state which recovers on timescales of nanoseconds to milliseconds. Charge separation takes place from the lowest exciton state, and the charge-separated state recovers to the lowest exciton state before emitting a delayed photon. The delayed emission exhibits power-law statistics very similar to those of the durations of bright and dark periods in blinking, suggesting a common origin. Indeed, we have successfully reproduced the delayed emission and the blinking statistics with a new blinking model, realising that there is in fact no uninterrupted optical cycling during bright periods. The power-law distribution of exciton recovery rates implies that charge-separated states have lifetimes ranging from μs to s. Short-living charge-separated states (μs) hardly affect the brightness of the QD, as long as the excitation rate is slower than the exciton recovery rate. Efforts

should mainly be aimed at reducing the effect of long-living charge-separated states (ms–s), because these lead to blinking and a resulting reduction in overall time-averaged brightness of the QD.

III. METHODS

Single quantum dot spectroscopy

For single-QD measurements the QDs were spin coated on a HMDS (hexamethyl disilazane) coated borosilicate glass coverslip from a dilute dispersion in toluene, and protected with a layer of spin-coated PMMA (polymethyl methacrylate). Single QDs were excited with supercontinuum light source (Fianium SC450) at a repetition rate of 1 MHz and a fluence of $\approx 10^{-4}$ J/cm^2. The excitation wavelength of 532 nm was selected by spectral filtering using an acousto-optical tunable filter (Crystal Technologies) and an additional short pass filter. Fluorescence light was collected through the same objective used for excitation, and separated from laser reflections using a long-pass filter with a cut-off at 590 nm. We used a Hanbury Brown-Twiss setup with two ID Quantique id100-20 ULN avalanche photo-diodes (APDs; dark counts < 10 Hz) connected to a timing card (DPC 230, Becker & Hickl GmbH) with 165 ps time resolution.

Monte Carlo simulation of the emission dynamics in a QD

The Monte Carlo simulation yielding the results of Fig. 4 is done as follows. First the initial state of the trap is set, i.e. the recovery rate γ_{R} and the 'stationary time' T until diffusion to a new state. A recovery rate is generated from a power-law distribution with exponent $\alpha_{\mathrm{R}} = 1.55$, a low-end cut-off of $1/10$ s and a high-end cut-off of $1/60$ ns (see Supplementary Figure S1). The stationary time is generated by first generating a trap diffusion rate γ_{d} from a power-law distribution with exponent $\alpha_{\mathrm{d}} = 1.7$, a low-end cut-off of $1/10$ s and a high-end cut-off of $1/60$ ns, and then T from an exponential distribution with decay constant γ_{d}. The QD is excited every 1 μs for a period of 5 min. Following each excitation, there is a probability of $P_{\mathrm{S}} = 15\%$ for charge carrier separation by trapping. If there is no separation (i.e. there is direct exciton recombination), a delay time t is simulated from an exponential distribution with decay constant $\gamma_{\mathrm{X}} = 1/30$ ns. If there is separation, the actual recovery rate γ_{R} is used to generate from an exponential distribution the time t until recovery of the delocalised exciton state and delayed emission. Optical cycling does not proceed until after the trapped carrier is released. When the stationary time T is exceeded, the trap state is reset by generating a new recovery rate γ_{R} and a new stationary time T as described above.

Fitting delayed emission dynamics

The normalised decay function due to a distribution of decay rates $\rho(\gamma) = \gamma^{\alpha-2}$ with an upper limit of γ_{max} is

$$I_{\mathrm{d}}(t) = \int_0^{\gamma_{\mathrm{max}}} \gamma\rho(\gamma)\mathrm{d}\gamma = \frac{\alpha-1}{\gamma_{\mathrm{max}}^{\alpha-1}}\, t^{-\alpha}\, \left[\Gamma(\alpha) - \Gamma(\alpha, \gamma_{\mathrm{max}} t)\right], \tag{1}$$

where $\Gamma(s)$ is the Gamma function, and $\Gamma(s,x)$ the incomplete Gamma function. Eq. 1 describes power-law $I_{\mathrm{d}} = t^{-\alpha}$ at long delay times $t \gg 1/\gamma_{\mathrm{max}}$, while the factor between square brackets is a correction to keep the function well-behaved at short times $t \approx 0$. In Supplementary Figure S1 we show that Eq. 1 with $\gamma_{\mathrm{max}} = \gamma_{\mathrm{X}}/2$ (where γ_{X} is the exciton decay rate) can be used as a good approximation for the delayed emission in case of back and forth charge separation and recovery of the exciton state. To fit the complete PL decay dynamics we use a model function with one (Fig. 4d) or two (Fig. 3a) components of the form:

$$I(t) = (1-P_{\mathrm{S}})\gamma_{\mathrm{X}}\mathrm{e}^{-\gamma_{\mathrm{X}}t} + P_{\mathrm{S}}\, \frac{\alpha-1}{(\gamma_{\mathrm{X}}/2)^{\alpha-1}}\, t^{-\alpha}\, \left[\Gamma(\alpha) - \Gamma(\alpha, \gamma_{\mathrm{X}} t/2)\right]. \tag{2}$$

The first term is the exponential contribution due to direct exciton recombination. The second term is the delayed contribution. In the Supplementary Figure S1 we explain that P_{S} must be interpreted as the probability of charge carrier separation for times longer than the intrinsic exciton lifetime $\tau_{\mathrm{X}} = 1/\gamma_{\mathrm{X}}$.

Estimating the PL quantum efficiency with the nanocrystal-cavity model

The rate of radiative decay γ_{rad} scales linearly with the local density of optical states experienced by an emitter. In a nanocrystal the local density of optical states depends on the refractive index of the surrounding solvent n, as described by the nanocrystal-

cavity model [23]:

$$\gamma_{\rm rad} \propto n \left(\frac{3n^2}{2n^2 + n_{\rm NC}^2} \right)^2 . \tag{3}$$

Here $n_{\rm NC}$ is the refractive index of the nanocrystal. We take $n_{\rm NC} = 2.5$, which is the refractive index for CdS around 600 nm [31]. The experimental exciton lifetimes $\tau_{\rm X}$ as a function of refractive index (Fig. 3b) are determined by a refractive-index dependent radiative component and a (presumably) fixed non-radiative component. We fit the data to

$$\tau_{\rm X} = \left[A\, n \left(\frac{3n^2}{2n^2 + n_{\rm NC}^2} \right)^2 + B \right]^{-1} , \tag{4}$$

where the first term describes radiative decay, and the second non-radiative decay. Using the fitted values of A and B the PL quantum efficiency $\eta(n)$ is calculated as

$$\eta(n) = 1 - B \left[A\, n \left(\frac{3n^2}{2n^2 + n_{\rm NC}^2} \right)^2 + B \right]^{-1} . \tag{5}$$

The solvents used are hexane ($n = 1.375$), cyclohexane ($n = 1.426$), chloroform ($n = 1.444$), trichloroethylene ($n = 1.478$), toluene ($n = 1.496$), chlorobenzene ($n = 1.524$), and carbon disulphide ($n = 1.627$).

Fitting emission spectra to a two-sided Gaussian

The emission spectra of Figs. 2c,d have an asymmetric shape, determined by the distribution of sizes and shapes in the ensemble. To fit the peak positions and band widths, we use two-sided Gaussian functions on energy (rather than wavelength) scale:

$$I(E) = A \begin{cases} {\rm e}^{-(E-E_0)^2/2\sigma_1^2} & ; \quad E < E_0 \\ {\rm e}^{-(E-E_0)^2/2\sigma_2^2} & ; \quad E > E_0 \end{cases} , \tag{6}$$

where A is the amplitude, E_0 the peak energy, σ_1 the width on the red side, and σ_2 the width on the blue side of the spectrum. In Fig. 2e we plot the peak positions E_0 and the full-widths-at-half-maximum $\sqrt{2\ln 2}(\sigma_1 + \sigma_2)$ of the emission spectra.

ACKNOWLEDGEMENTS

This work is part of the research program of the 'Stichting voor Fundamenteel Onderzoek der Materie (FOM)', which is financially supported by the 'Nederlandse Organisatie voor Wetenschappelijk Onderzoek (NWO)'.

[1] Frantsuzov, P., Kuno, M., Jankó, B. & Marcus, R. A. Universal emission intermittency in quantum dots, nanorods and nanowires, *Nat. Phys.* **4**, 519-522 (2008)

[2] Cordones, A. A. & Leone, S. R. Mechanisms for charge trapping in single semiconductor nanocrystals probed by fluorescence blinking, *Chem. Soc. Rev.* **42**, 3209–3221 (2013)

[3] Nirmal, M. *et al.* Fluorescence intermittency in single cadmium selenide nanocrystals, *Nature* **383**, 802-804 (1996)

[4] Efros, Al. L. & Rosen, M. Random telegraph signal in the photoluminescence intensity of a single quantum dot, *Phys. Rev. Lett.* **78**, 6, 1110-1113 (1997)

[5] Kuno, M., Fromm, D. P., Hamann, H. F., Gallagher, A. & Nesbitt, D. J. 'On'/'off' fluorescence intermittency of single semiconductor quantum dots, *J. Chem. Phys.* **115**, 1028–1040 (2001)

[6] Verberk, R., Van Oijen, A. M. & Orrit, M. Simple model for the power-law blinking of single semiconductor nanocrystals, *Phys. Rev. B* **66**, 233202 (2002)

[7] Tang, J. & Marcus, R. A. Mechanisms of fluorescence blinking in semiconductor nanocrystal quantum dots, *J. Chem. Phys.* **123**, 054704 (2005)

[8] Rosen, S., Schwartz, O. & Oron, D. Transient fluorescence of the off state in blinking CdSe/CdS/ZnS semiconductor nanocrystals is not governed by Auger recombination, *Phys. Rev. Lett.* **104**, 157404 (2010)

[9] Zhao, J., Nair, G., Fisher, B. R. & Bawendi, M. G. Challenge to the charging model of semiconductor-nanocrystal fluorescence intermittency from off-state quantum yields and multiexciton blinking, *Phys. Rev. Lett.* **104**, 157403 (2010)

[10] Cordones, A. A., Bixby, T. J. & Leone, S. R. Direct measurement of off-state trapping rate fluctuations in single quantum dot fluorescence, *Nano Lett.* **11**, 3366-3369 (2011)

[11] Frantsuzov, P. A. & Marcus, R. A. Explanation of quantum dot blinking without the long-lived trap hypothesis, *Phys. Rev. B* **72**, 155321 (2005)

[12] Frantsuzov, P. A., Volkán-Kacsó, S. & Jankó, B. Model of fluorescence intermittency of single colloidal semiconductor quantum dots using multiple recombination centers, *Phys. Rev. Lett.* **103**, 207402 (2009)

[13] Frantsuzov, P. A., Volkán-Kacsó, S. & Jankó, B. Universality of the fluorescence intermittency in nanoscale systems: experiment and theory, *Nano Lett.* **13**, 402–408 (2013)

[14] Galland, C. *et al.* Two types of luminescence blinking revealed by spectroelectrochemistry of single quantum dots, *Nature* **479**, 203-207 (2011)

[15] Qin, W. & Guyot-Sionnest, P. Evidence for the role of holes in blinking: negative and oxidized CdSe/CdS dots, *ACS Nano* **6**, 10, 9125-9132 (2012)

[16] Sher, P. H., Smith, J. M., Dalgarno, P. A., Warburton, R. J., Chen, X., Dobson, P. J., Daniels, S. M., Pickett, N. L. & O'Brien, P. Power law carrier dynamics in semiconductor nanocrystals at nanosecond timescales, *Appl. Phys. Lett.* **92**, 101111 (2008)

[17] Jones, M., Lo, S. S. & Scholes, G. D. Quantitative modeling of the role of surface traps in CdSe/CdS/ZnS nanocrystal photoluminescence decay dynamics, *Proc. Natl. Acad. Sci. U. S. A.* **106**, 3011–3016 (2009)

[18] Bharadwaj, P. & Novotny, L. Robustness of quantum dot power-law blinking, *Nano Lett.* **11**, 2137–2141 (2011)

[19] Gómez, D. E., Van Embden, J., Mulvaney, P., Fernée, M. J. & Rubinsztein-Dunlop, H. Exciton-trion transitions in single CdSe-CdS core-shell nanocrystals, *ACS Nano* **3**, 8, 2281-2287 (2009)

[20] Spinicelli, P. *et al.* Bright and grey states in CdSe-CdS nanocrystals exhibiting strongly reduced blinking, *Phys. Rev. Lett.* **102**, 136801 (2009)

[21] Galland, C. *et al.* Lifetime blinking in nonblinking nanocrystal quantum dots, *Nat. Commun.* **3**, 908 (2012)

[22] Van Driel, A. F., Allan, G., Delerue, C., Lodahl, P., Vos, W. L. & Vanmaekelbergh, D., Frequency-dependent spontaneous emission rate from CdSe and CdTe nanocrystals: influence of dark states, *Phys. Rev. Lett.* **95**, 236804 (2005)

[23] Senden, T., Rabouw, F. T. & Meijerink, A. Photonic effects on the radiative decay rate and luminescence quantum yield of doped nanocrystals, *ACS Nano* **9**, 1801–1808 (2015)

[24] Rabouw, F. T., Den Hartog, S. A., Senden, T. & Meijerink, A. Photonic effects on the Förster resonance energy transfer efficiency, *Nat. Commun.* **5**, 3610 (2014)

[25] Park, Y.S., Bae, W. K., Pietryga, J. M. & Klimov, V. I. Auger recombination of biexcitons and negative and positive trions in individual quantum dots, *ACS Nano* **8**, 7288–7296 (2014)

[26] Javaux, C. *et al.* Thermal activation of non-radiative Auger recombination in charged colloidal nanocrystals, *Nat. Nanotechnol.* **8**, 206–212 (2013)

[27] Rabouw, F. T. *et al.* Reduced Auger recombination in single CdSe/CdS nanorods by one-dimensional electron delocalization, *Nano Lett.* **13**, 4884–4892 (2013)

[28] Jha, P. P. & Guyot-Sionnest, P. Trion decay in colloidal quantum dots, *ACS Nano* **3**, 1011–1015 (2009)

[29] Cohn, A. W., Rinehart, J. D., Schimpf, A. M., Weaver, A. L. & Gamelin, D. R. Size dependence of negative trion Auger recombination in photodoped CdSe nanocrystals, *Nano Lett.* **14**, 353–358 (2014)

[30] Cohn, A. W., Schimpf, A. M., Gunthardt, C. E. & Gamelin, D. R. Size-dependent trap-assisted Auger recombination in semiconductor nanocrystals, *Nano Lett.* **13**, 1810–1815 (2013)

[31] Jensen, B. & Torabit, A. Refractive index of hexagonal II-VI compounds CdSe, CdS, and $CdSe_xS_{1-x}$, *J. Opt. Soc. Am. B* **3**, 857–863 (1986)

Supplementary information to
Delayed exciton emission and its relation to blinking in CdSe quantum dots

Freddy T. Rabouw,[1] Marko Kamp,[2] Relinde J. A. van Dijk-Moes,[1] Daniel R. Gamelin,[3] A. Femius Koenderink,[2] Andries Meijerink,[1] and Daniël Vanmaekelbergh[1]

[1] *Condensed Matter and Interfaces, Debye Institute for Nanomaterials Science, Princetonplein 1, 3584 CC Utrecht, The Netherlands*
[2] *Center for Nanophotonics, FOM Institute AMOLF, Science Park 104, 1098 XG Amsterdam, The Netherlands*
[3] *Department of Chemistry, University of Washington, Seattle, Washington 98195–1700, United States*

Synthesis of CdSe/CdS/CdZnS/ZnS core–multi-shell QDs following Ref. [1]
Relinde please provide numbers specific for synthesis RM877

Chemicals. $Cd(Ac)_2$ (Sigma-Aldrich, 99%), diethylzinc (Et_2Zn, Sigma Aldrich, 1.0 M solution in hexane), Oleic acid (OA, Sigma-Aldrich, 90%), octadecene (ODE, Sigma-Aldrich, 90%), octadecene amine (ODA, Sigma-Aldrich, 90%) selenium (Strem Chemicals, 99.99%), sulphur (Alfa Aesar, 99%), trioctylphosphine (TOP, Sigma-Aldrich, 90%), trioctylphosphine oxide (TOPO, Sigma-Aldrich, 99%), were used for the synthesis of nanoparticles (NPs).

Solvents. Acetone (Merck), cyclohexane (Sigma-Aldrich, anhydrous, 99%), hexane (Sigma-Aldrich, anhydrous, 99.8%), methanol (Sigma-Aldrich, anhydrous, 99.8%), toluene (Sigma-Aldrich, anhydrous, 99.8%).

Precursor preparation. Cadmium precursor I [0.1 M $Cd(OA)_2$] was prepared by mixing OA (3.68 g), ODE (25.92 g) and $Cd(Ac)_2$ (0.64 g), and heating to 150°C under vacuum for 2 h. Cadmium precursor II [0.1 M $Cd(OA)_2$] was prepared by dissolving $Cd(Ac)_2$ (1.10 g) in OA (10.83 g) and ODE (43.20 mL), and heating to 150°C under vacuum for 2 h. Selenium precursor was prepared by dissolving elemental selenium (4.25 g) in TOP (22.5 g) at 50C, followed by the addition of ODE (35.7 g). Zinc precursor [0.1 M $Zn(OA)_2$] was prepared by dissolving $Zn(Et)_2$ (0.494 g) in OA (5.05 mL) and ODE (19.8 mL) at 310°C. Sulphur precursor solution (0.1 M) was prepared by dissolving sulphur (0.032 g) in ODE (10 mL) at 180 C.

Synthesis of CdSe nanocrystal seeds. CdSe nanocrystal seeds were synthesized in 50 ml three-neck flask using a Schlenk-line. TOPO (1.11 g), ODA (3.20 g), and $Cd(OA)_2$-precursor (4.9 g) were mixed, heated to 300°C. When this temperature was reached, the Se precursor (5.2 g) was added rapidly. The mixture was cooled down after XXX s. The particles were diluted by adding 1 equivalent of hexane. The quantum dots were washed by adding 2 equivalents of methanol and collecting the upper hexane layer (coloured) and add 1 equivalent of acetone to precipitate the QDs. Finally, the nanocrystal seeds were dissolved in toluene.

CdS/CdZnS/ZnS shell growth. The Cd-, Zn-, and Cd/Zn-precursor solutions were kept at about 80°C, while the sulphur injection solution was allowed to cool to room temperature. For each shell growth, a calculated amount of a given precursor solution was injected with a syringe using standard air-free procedures. CdSe QDs (10^{-7} M of QDs with 3.4 nm diameter in toluene), ODE (5.0 g) and ODA (1.5 g) were mixed and heated up to 150°C for 1 h to remove all toluene. The reaction temperature was increased to 240°C and in steps with reaction periods of 30 minutes the precursors were added slowly to grow the shell layer-by-layer.

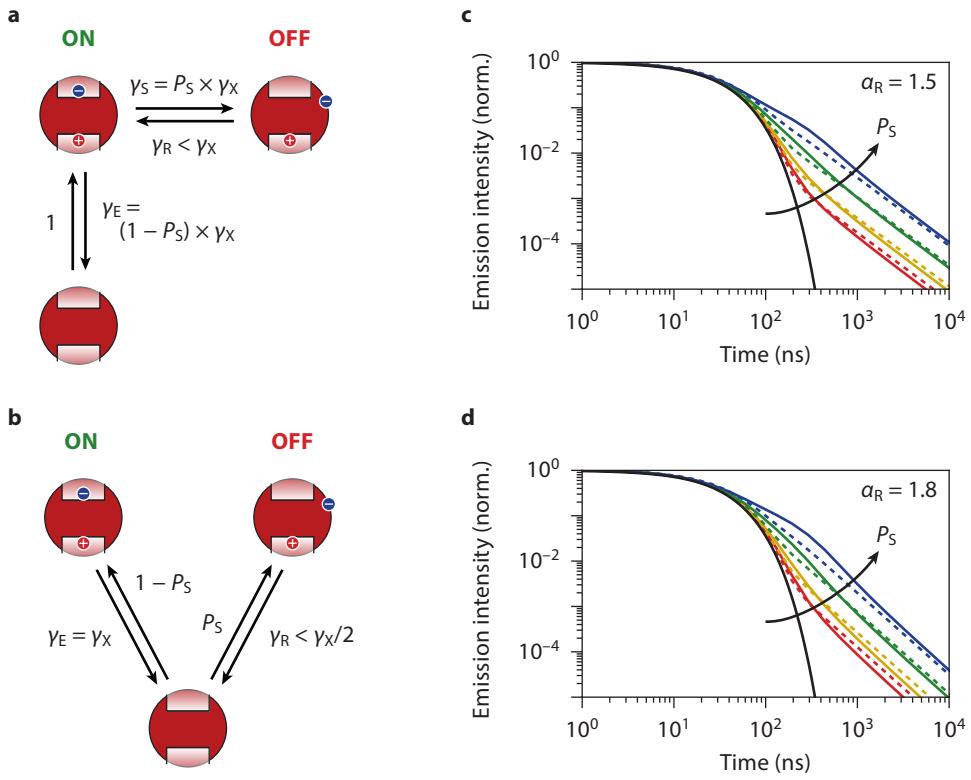

Supplementary Figure S1 — Photoluminescence decay following charge carrier trapping, storage and release.

Power-law decay contains an infinite number of exponents. To get a power-law decay of the delayed emission $I(t) \propto t^{-\alpha_R}$ at long timescales the exciton recovery rates should be distributed as

$$\rho(\gamma_R) = \begin{cases} \gamma_R^{\alpha_R - 2} & ; \ \gamma_R < \gamma_{max} \\ 0 & ; \ \gamma_R > \gamma_{max} \end{cases}, \tag{1}$$

where the upper limit γ_{max} in rates is imposed to avoid a singularity at $t = 0$. This leads to decay dynamics of

$$I(t) = \int_0^{\gamma_{max}} \gamma_R \, \rho(\gamma_R) e^{-\gamma_R t} \, d\gamma_R = [\Gamma(\alpha_R) - \Gamma(\alpha_R, \gamma_{max} t)] \, t^{-\alpha_R}, \tag{2}$$

where the factor between square brackets describes the correction at short times to ensure that the function is well-behaved. To obtain power-law PL decay for the delayed component in our simulation, we make sure that the distribution of release rates of the trapped charge follows Eq. 1. Hence for $\alpha_R < 2$, although very long periods of charge separation are rare, the probability of occurrence per unit of recovery rate is actually higher for slow rates $\gamma_R \approx 0$ than for fast rates $\gamma_R \approx \gamma_{max}$.
The difficulty now lies in the choice for γ_{max}. In principle, there is no reason to assume that the recovery rates are widely (power-law) distributed from s^{-1} to ns^{-1}, but that there is some finite upper limit. However, we can make use of the fact that if at a certain point in time a trap is active with a recovery rate of order ns^{-1} or faster, it will hardly affect the dynamics of photon emission. More precisely, in that case the rate limiting step is the emission process itself, not detrapping and recovery of the delocalised exciton state. The charge-separated state is formed on a timescale of $1/\gamma_X$ (where $\gamma_X = \gamma_E + \gamma_S$ is the total decay rate of the exciton), recovers to the delocalised exciton on a timescale of $1/\gamma_R$, which then emits on a timescale of $1/\gamma_X$. Hence, the shortest possible time scale of delayed emission $2/\gamma_X$.

(a) The kinetic scheme of charge carrier trapping, storage and release. The corresponding three-level rate equation model containing individual rates is

$$\frac{dN_X}{dt} = -\gamma_X N_X(t) + \gamma_R N_S(t) \tag{3}$$

$$\frac{dN_S}{dt} = \gamma_S N_X(t) - \gamma_R N_S(t) \tag{4}$$

$$N_X(0) = 1 \tag{5}$$

$$N_S(0) = 0, \tag{6}$$

where t is the delay time after excitation, N_{X} the population of the exciton state, and N_{S} the population of the charge-separated state. This system of equations can be solved to yield the time evolution of the population in the exciton state $N_{\mathrm{X}}(t)$. In our model the values of γ_{X} and γ_{S} are fixed, while γ_{R} varies on long timescales sampling a power-law distribution. The theoretical PL decay curve $I(t)$ is obtained by integrating over the distribution of recovery rates:

$$I(t) = \gamma_{\mathrm{E}} \langle N_{\mathrm{X}}(t) \rangle = \gamma_{\mathrm{E}} \int_0^{\gamma_{\mathrm{max}}} \rho(\gamma_{\mathrm{R}}) N_{\mathrm{X}}(t) \, \mathrm{d}\gamma_{\mathrm{R}}. \tag{7}$$

We take $\gamma_{\mathrm{max}} = \gamma_{\mathrm{X}}$, i.e. we consider only release rates slower than γ_{X}. This choice reflects that only such relatively slow release rates can lead to emission that is clearly delayed compared to normal exciton emission. $N_{\mathrm{X}}(t)$ describes the population decay of the exciton state which is dependent of all rate constants including γ_{R}.

(b) A much simpler model where a fraction $P_{\mathrm{S}} = \gamma_{\mathrm{S}}/\gamma_{\mathrm{X}}$ of the photons are contained in the delayed emission component, with a power-law distributed rate having $\gamma_{\mathrm{max}} = \gamma_{\mathrm{X}}/2$. The factor 1/2 here accounts for the fact that a pathway leading to delayed emission goes through the exciton state with decay rate γ_{X} (at least) twice, as discussed above. The power-law decay of the trapped state is as described by Eq. 2. The rest (fraction $1 - P_{\mathrm{S}}$) of the photons are emitted from the exciton state and contribute an exponential component with decay constant γ_{X}. The total PL decay should follow

$$I(t) = (1 - P_{\mathrm{S}}) \gamma_{\mathrm{X}} \mathrm{e}^{-\gamma_{\mathrm{X}} t} + P_{\mathrm{S}} (\alpha_{\mathrm{R}} - 1) \gamma_{\mathrm{max}}^{1-\alpha_{\mathrm{R}}} \left[\Gamma(\alpha_{\mathrm{R}}) - \Gamma(\alpha_{\mathrm{R}}, \gamma_{\mathrm{max}} t) \right] t^{-\alpha_{\mathrm{R}}} \tag{8}$$

(c,d) The normalized PL decay trace in case of power exponents of **(c)** $\alpha_{\mathrm{R}} = 1.5$ or **(d)** $\alpha_{\mathrm{R}} = 1.8$ for the recovery rates, at different trapping probabilities of $P_{\mathrm{S}} = 0\%$ (black), 5% (red), 10% (yellow), 25% (green), and 50% (blue), and simulated with the three-level rate equation model (solid lines; Fig. S1a, Eq. 7) or with the simpler model (dashed lines; Fig. S1b, Eq. 8). We took $\gamma_{\mathrm{X}} = 1/30$ ns.

Since there is a good correspondence between the two models, we conclude that we can use the analytical expression from the simplified model (Fig. S1b, Eq. 8) to fit the decay dynamics of QD PL under the influence of charge carrier trapping, storage and release. The parameter P_{S} must be interpreted as the probability of charge separation due to charge carrier trapping in a trap with a release rate slower than the intrinsic exciton decay rate ($\gamma_{\mathrm{R}} < \gamma_{\mathrm{X}}$), since only such traps are considered in the rate-equation model (Fig. S1a, Eq. 7).

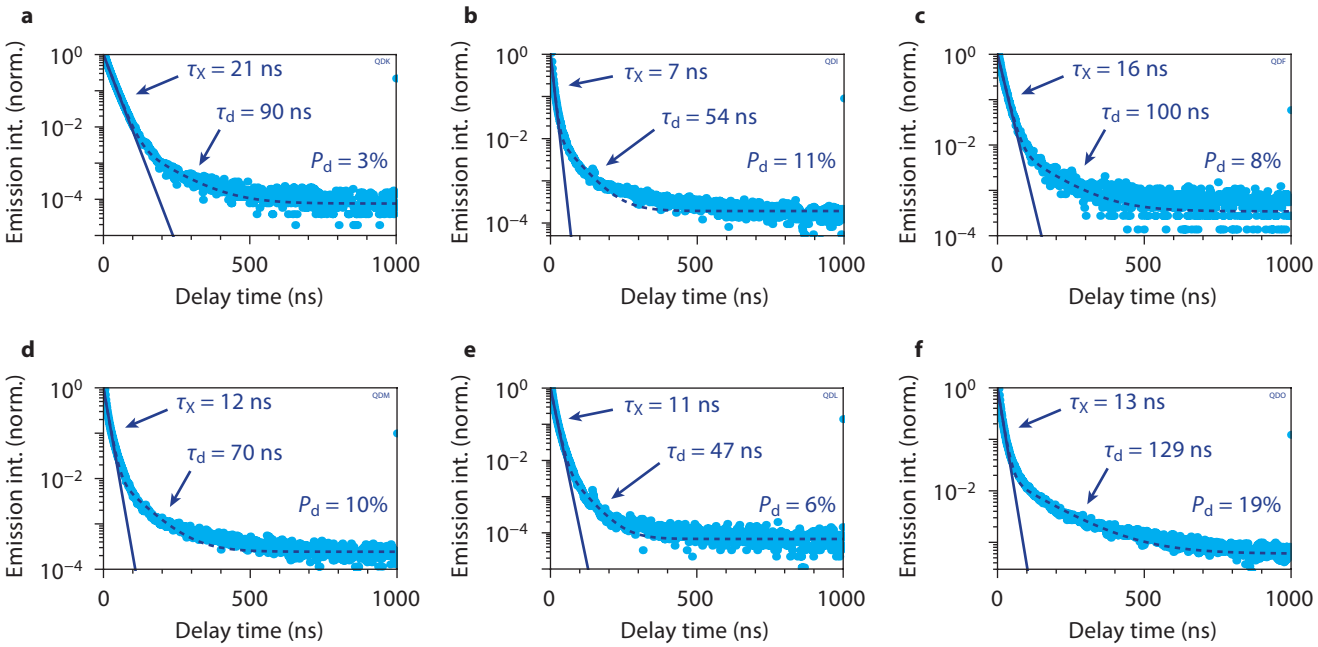

Supplementary Figure S2 — Delayed emission in the PL decay of single core–shell quantum dots.

(a–f) PL decay curves of six single core–shell QDs. The exciton lifetime τ_X is estimated from a single-exponential fit to the first 100 ns. At longer timescales, typically at a normalised intensity of 10^{-3}–10^{-2}, the decay deviates from this single exponential. A 'delayed component' and a background is added, from which we obtain a 'delayed lifetime' τ_d and the relative contribution of the delayed component $P_d = A_d\tau_d/(A_X\tau_X + A_d\tau_d)$ (where A_X and A_d are the amplitudes of the direct and the delayed component). The fitted values for τ_X, τ_d and P_d are given each panel. The values for P_d are underestimated because part of the delayed contribution is hidden by the background noise with a relative intensity of 10^{-4}–10^{-3}. Indeed, the absolute count rates of the fitted 'background' [which are (**a**) 4, (**b**) 14, (**c**) 3, (**d**) 17, (**e**) 6, and (**f**) 18 counts per time bin of 1.65 ns over a 5 min measurement] show a correlation with with delayed contribution P_d, indicating that the 'background' consists in part of delayed photons. We see that a delayed component is apparent in the PL decay of all single QDs, but the relative contribution varies from QD to QD.

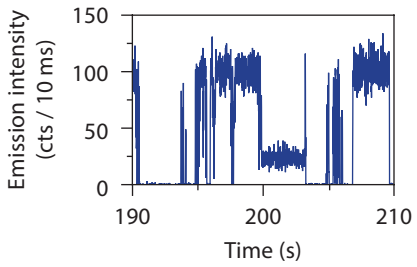

Supplementary Figure S3 — Discussion of B-type blinking in terms of our new blinking model.

Recently, Galland *et al.* [2] observed what they called 'B-type blinking': the QD blinks between a bright state and state with lower intensity but the same PL decay rate. B-type blinking was ascribed to hot-electron capture, which explains that while traps are active fewer excitations cool down to a ground state exciton (hence the lower intensity) but that the lowest exciton state itself is not affected (hence the unaffected PL decay rate). An alternative explanation of B-type blinking, not involving the scenario of hot-electron capture, would be that in their experiment a type of charge carrier trap is introduced (perhaps in the electrode used) that can make a charge-separation state with a recovery rate γ_{R} on the order of the excitation rate of the QD. If such trap were active, the QD would exhibit ON durations of on average $\langle T_{\mathrm{ON}} \rangle = 1/P_{\mathrm{S}}\gamma_{\mathrm{exc}}$ (with γ_{exc} the excitation rate of the QD) and OFF durations of on average $\langle T_{\mathrm{OFF}} \rangle = 1/\gamma_{\mathrm{R}}$. Averaged over a time bin in the intensity trace, the apparent quantum efficiency the active period of the trap would be $\eta = \langle T_{\mathrm{ON}} \rangle / (\langle T_{\mathrm{ON}} \rangle + \langle T_{\mathrm{OFF}} \rangle) = \gamma_{\mathrm{R}}/(P_S\gamma_{\mathrm{exc}} + \gamma_{\mathrm{R}})$. An apparent quantum efficiency η would correspond to an exciton recovery rate of $\gamma_{\mathrm{R}} = P_S\gamma_{\mathrm{exc}}\eta/(1-\eta)$.

The plot is a zoom-in of the intensity trace of Fig. 3b in the main text, as simulated with our model. It shows a period between 199 s to 203 s where the intensity is at some intermediate level between the brightest state and the darkest state. Note that in our model the OFF state is completely dark, so that intermediate intensities must be due to rapid switching between ON and OFF on timescales faster than the binning time of the intensity trace. The rate of switching is determined by the recovery rate γ_{R}, which can be fixed for a long period T. The intermediate intensity state occurring around $t = 200$ s, with an apparent quantum efficiency of $\eta \approx 25\%$ occurs because during these 4 s the trap has a release rate of $\gamma_{\mathrm{R}} \approx 0.05\ \mu\mathrm{s}^{-1}$.

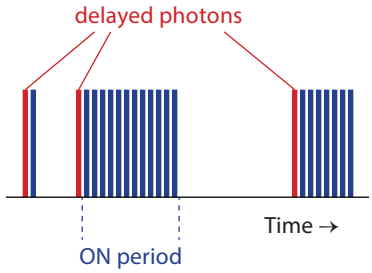

Supplementary Figure S4 — The delayed contribution in existing blinking models.

We investigate what would be the integrated contribution of delayed emission if we assume, as done in existing blinking models, that ON periods are characterised by uninterrupted optical cycling. We further assume that each laser pulse leads to the absorption of a photon in the QD. The situation would be as in the cartoon. It shows the photon emission from a QD with an exciton lifetime of $\tau = 30$ ns that is excited every time bin of, say, 100 ns. There are ON periods during which each excitation leads to exciton emission (blue bars; uninterrupted optical cycling). Every now and then there is charge carrier separation, after which the QD is dark. At some moment in time the exciton state recovers and emits a delayed photon (red bars). Optical cycling then continues. If the ON periods are power-law distributed (Fig. 1 in the main text, as well as in many other QD samples [3, 4]) and we assume that during ON periods there is only direct exciton emission due to uninterrupted optical cycling, then the contribution of delayed emission can be calculated using the following reasoning.

The contribution of delayed emission is simply the fraction of bars in the diagram that is red. Clearly, every long-lived ON period (say, longer than a ms) would be a huge decrease of the relative number of red bars. The fraction of bars that is red, i.e. the contribution of delayed emission, is calculated as

$$P_{\mathrm{d}} = \frac{\int_{t_{\mathrm{min}}}^{t_{\mathrm{max}}} t^{-\alpha}\,\mathrm{d}t}{t_{\mathrm{min}}^{-1}\int_{t_{\mathrm{min}}}^{t_{\mathrm{max}}} t\,t^{-\alpha}\,\mathrm{d}t}. \tag{9}$$

Here the integrations are over all possible durations of ON periods, which range from t_{min} (the repetition period of the laser, which defines the time resolution) to t_{max} (the longest possible ON duration). In the numerator we consider that each possible ON duration contains only a single delayed photon (namely the first; see cartoon). In the denominator we have the total number of photons $t_{\mathrm{min}}^{-1}t$ emitted during an ON period with duration t.

With reasonable values of $t_{\mathrm{min}} = 100$ ns, $t_{\mathrm{max}} = 10$ s, and $\alpha = 1.6$, we get a predicted delayed contribution of $P_{\mathrm{d}} = 4 \times 10^{-4}$. This value is far off from the experimental contribution of approximately 10% (Fig. 3c in the main text, and Supplementary Fig. S2). Clearly, the assumption that ON periods involve uninterrupted optical cycling is inconsistent with our data.

[1] Xie, R., Kolb, U., Li, J., Basch, T. & Mews, A. Synthesis and characterization of highly luminescent CdSe–core CdS/$Zn_{0.5}Cd_{0.5}$S/ZnS multishell nanocrystals, *J. Am. Chem. Soc.* **127**, 7480–7488 (2005)

[2] Galland, C. *et al.* Two types of luminescence blinking revealed by spectroelectrochemistry of single quantum dots, *Nature* **479**, 203-207 (2011)

[3] Kuno, M., Fromm, D. P., Hamann, H. F., Gallagher, A. & Nesbitt, D. J. 'On'/'off' fluorescence intermittency of single semiconductor quantum dots, *J. Chem. Phys.* **115**, 1028–1040 (2001)

[4] Cordones, A. A. & Leone, S. R. Mechanisms for charge trapping in single semiconductor nanocrystals probed by fluorescence blinking, *Chem. Soc. Rev.* **42**, 3209–3221 (2013)